Thermal Switching between Blue and Red Luminescence in Magnetic Chiral Cyanido-Bridged Eu^{III}-W^{V} Coordination Helices

Szymon Chorazy,[a,b] Koji Nakabayashi,[a] Noriaki Ozaki,[a] Robert Pełka,[c] Tomasz Fic,[d] Jacek Mlynarski,[b] Barbara Sieklucka*[b] and Shin-ichi Ohkoshi*[a,e]

[a]Department of Chemistry, School of Science, The University of Tokyo, 7-3-1 Hongo, Bunkyo-ku, Tokyo, 113-0033, Japan. E-mail: ohkoshi@chem.s.u-tokyo.ac.jp (S. Ohkoshi), [b]Faculty of Chemistry, Jagiellonian University, Ingardena 3, 30-060 Kraków, Poland, [c]H.Niewodniczański Institute of Nuclear Physics PAN, Radzikowskiego 152, 31-342 Kraków, Poland, [d]Institute of Physics, Jagiellonian University, Reymonta 4, 30-059 Kraków, Poland, [e]CREST, JST, K's Gobancho, 7 Gobancho, Chidoya-ku, Tokyo, 102-0076, Japan

1. Experimental details.

1a. Materials

$TBA_3[W(CN)_8]$ was synthesized according to the published procedure.[S1] (*RR*)- and (*SS*)-Pr^i-Pybox, $Eu(NO_3)_3 \cdot 6H_2O$ and all solvents were purchased from Tokyo Chemical Industry or Wako Chemicals GmbH and used without purification.

1b. Synthesis of 1-(*RR*) and 1-(*SS*)

1-(*RR*): The mixed solution of acetonitrile, methanol and N,N-dimethylformamide (2:2:1, v/v/v) was used as a solvent. $Eu(NO_3)_3 \cdot 6H_2O$ (0.02 mmol) and (RR)-Pr^i-pybox (0.08 mmol) were dissolved in 2.0 mL of solvent. Then $TBA_3[W(CN)_8]$ (0.02 mmol) dissolved in 1.0 mL of solvent was added and solution were layered by diethyl ether. Needle crystals of **1**-(RR)·dmf·$4H_2O$ appeared after three days. Suction filtration and air-drying gave the polycrystalline solid of **1**-(*RR*). Yield 15.2 mg, 63%. IR (KBr, cm^{-1}). CN$^-$ stretching vibrations: 2168m, 2161w, 2147w, 2138w. Anal. (ICP-MS, CHN analysis). Calcd. for $Eu_3W_3C_{114}H_{176}N_{46}O_{27}$: Eu, 12.56%; W, 15.19%; C, 37.72%; H, 4.89%; N, 17.75%. Found: Eu, 12.44%; W, 15.36%; C, 37.57%; H, 4.89%; N, 17.62%.

The synthesis of **1**-(*SS*) was analogous to the synthesis of **1**-(*RR*) using (*SS*)- Pr^i-pybox instead of (*RR*)- Pr^i-pybox. Yellow needle crystals of **1**-(*SS*)·dmf·$4H_2O$ appeared after few days. Suction filtration and air-drying gave the polycrystalline solid of **1**-(*SS*). Yield 16.0 mg, 67%. IR (KBr, cm^{-1}). CN$^-$ stretching vibrations: 2169m, 2161w, 2148w, 2138w. Anal. (ICP-MS, CHN analysis). Calcd. for $Eu_3W_3C_{114}H_{176}N_{46}O_{27}$: Eu, 12.56%; W, 15.19%; C, 37.72%; H, 4.89%; N, 17.75%. Found: Eu, 12.36%; W, 15.33%; C, 37.46%; H, 4.90%; N, 17.62%.

TGA for **1**-(*RR*) and **1**-(*SS*) (Fig. S1): 20-60°C – weight loss of 4.0% (-$8H_2O$), 100-120°C – 8.0% (-4dmf) , above 190°C – 50% (-CN$^-$ and -dmf).

1b. Crystal structure determination

Single crystal diffraction data of **1**-(*RR*) and **1**-(*SS*) were collected on a Rigaku R-AXIS RAPID imaging plate area detector with graphite monochromated Mo Kα radiation. The single crystals were dispersed in paratone-N oil, mounted on Micro Mounts™ and measured at 90(2)K. The crystal structures were solved by a direct method and refined by a full-matrix least-squares technique using SHELXL-97 and SHELXH-97.[S2] Calculations were performed using partly Crystal Structure crystallographic software package and partly WinGX (ver. 1.80.05) integrated system.[S3] Non-hydrogen atoms were refined anisotropically while the hydrogen atoms were refined using the riding model. Part of carbon atoms of some dmf molecules was structurally disordered and two

crystallographic positions with the fractional occupancy were proposed. Methanol and water solvent molecules were highly disordered and the fractional occupancy and restraints on their thermal ellipsoids were introduced during the refinement procedure. Structural diagrams were prepared using Mercury 1.2.3. software.

1c. Physical techniques

IR spectra were recorded on JASCO FTIR-4100 spectrometer in the 4000-400 cm^{-1} range on KBr discs. Elemental analyses of Eu and W were measured by Agilent 7700 Series inductively coupled plasma mass spectrometer (ICP-MS) while those of C, H, N were determined by standard microanalytical methods. Thermogravimetric measurements were conducted by RIGAKU Thermo Plus TG8120 at a heating rate of 2°C per minute. The UV-Vis diffuse reflectance spectra were measured by a Shimadzu UV-3100 spectrometer on the powder samples mixed with barium sulphate. CD spectra were measured on the powder sample dispersed in nujol using JASCO J-810 spectropolarimeter.

Magnetic measurements were carried out using a superconducting quantum interference device (SQUID) magnetometer (Quantum Design, MPMS-7) in the 2-300 K range. The magnetic susceptibility data were corrected for the diamagnetic contribution using Pascal constants.[S4-S5]

Emission and excitation spectra were measured on Hitachi Fluorescence Spectrophotometer F-4500 using FL Solutions program. Both room temperature as well as low temperature emission and excitation spectra were recorded in emission mode with 240 nm/min scan speed, 10 nm excitation slit, 1 nm emission slit and 400 V voltage of photomultiplier detector. Time scan for the determination of luminescence lifetime were executed in Phosphorescence Short Life Time data mode with fixed 40 μs data sampling interval. 10 nm excitation slit, 5 nm emission slit and 700 V voltage of photomultiplier detector were used. The calculation of the phosphorescence life time was performed using automatic option embedded in the software. Low temperature measurement was executed at 77 K in the cryostat filled by liquid nitrogen. It is important to note that the sample of **1**-(*RR*) was sensitive to the UV light used as an excitation source. During the long irradiation by strong UV light the intensity of the whole emission spectrum gradually decreased which is probably due to the UV-induced photoreactivity connected with the reduction of W^V as was observed also for other luminescent systems based on lanthanide ions and octacyanidotungstate(V).[S6]

1d. Calculations

Continuous Shape Measure Analysis for coordination spheres of eight-coordinated W(V) and nine-coordinated Eu(III) ions was performed by SHAPE software ver. 1.1b[S7-S9].

2. Details concerning the calculations of magnetic properties of **1**-(*RR*) and **1**-(*SS*)

The ^{7}F ground term of the Eu^{III} ion is split by the spin-orbit coupling into seven states ^7F_J with J taking the integer values from 0 to 6. The spin orbit coupling operator reads $H_{SO} = \lambda \boldsymbol{L} \cdot \boldsymbol{S}$, where λ is the spin-orbit coupling constant. The energies of the states are $E(J) = \lambda J(J+1)/2$ where the energy of the $^7F_0$ ground state is taken as the origin. Despite the ground state being diamagnetic there is nonzero contribution to the magnetic susceptibility. This is due to the fact that λ is small enough for the first excited states to be thermally populated.[S4] The molar magnetic susceptibility may be expressed as

$$\chi_{Eu} = \frac{\sum_{J=0}^{6}(2J+1)\chi(J)\exp[-\lambda J(J+1)/2k_BT]}{\sum_{J=0}^{6}(2J+1)\exp[-\lambda J(J+1)/2k_BT]}$$

where

$$\chi(J) = \frac{N_A\mu_B^2 g_J^2 J(J+1)}{3k_BT} + \frac{2N_A\mu_B^2(g_J-1)(g_J-2)}{3\lambda}$$

N_A denotes the Avogadro number, μ_B is the Bohr magneton, k_B - the Boltzmann constant, and $g_J = 3/2$ for $J \neq 0$ and $g_J = 5$ for $J = 0$. The first term in the above formula is the standard contribution from a non-interacting magnetic center with spin quantum number J and the Landé factor g_J, whereas the second term represents a temperature independent second order quantum correction due to the presence of excited states not too far in energy from the ground state. Because the ground state of Eu^{III} ion is diamagnetic we can with a good approximation neglect the magnetic coupling with the adjacent W^V ions and treat both centers independently. The contribution to the molar magnetic susceptibility from the tungsten center is a free-ion one and is calculated with the formula

$$\chi_W = \frac{N_A\mu_B^2 g_W^2 S_W(S_W+1)}{3k_BT}$$

where g_W is the Landé factor of the W^V ion and S=1/2.

The total molar magnetic susceptibility corresponding to the Eu_3W_3 unit of **1**-(*RR*) and **1**-(*SS*) is calculated as the following sum $\chi_{total} = 3(\chi_{Eu} + \chi_W)$, which has been implemented into the fitting procedure.

At low temperatures the population of the excited states is negligible, so the only contribution to the magnetization comes from the non-interacting W^V centers and is given by the following formula

$$M = 3N_A \mu_B g_W S_W \tanh\left(\frac{g_W \mu_B S_W H}{k_B T}\right).$$

The fitting procedure gives a spin-orbit coupling constant of Eu^{III} ions and a g-value of W^V ions. These values are averaged as the real complication in investigated systems comes from their non-trivial crystal structure. The main structural unit comprises a chain where Eu^{III} ion alternates with the W^V ion. The periodically repeating chain unit does not simply contain a single Eu^{III}-W^V pair, but a triple of such pairs indicating the presence of three Eu^{III} differing in their coordination spheres and hence in their magnetic properties. A full model should take this structural complication duly into account. However, it necessarily will introduce overparametrization, which given only the powder data measurements at hand poses a complex and rather unresolvable problem. Therefore, we take here a simpler approximated approach in which we treat all the Eu^{III} ions as equivalent. This requires a single averaged spin-orbit coupling constant in the calculations.

The g-values obtained from the simulation of magnetic data are comparable to g-values determined by ESR spectroscopy (not shown). ESR spectra reveal slightly lower value ($g_W = 1.94(1)$) and do not show the noticeable difference between **1**-(*RR*) and **1**-(*SS*).
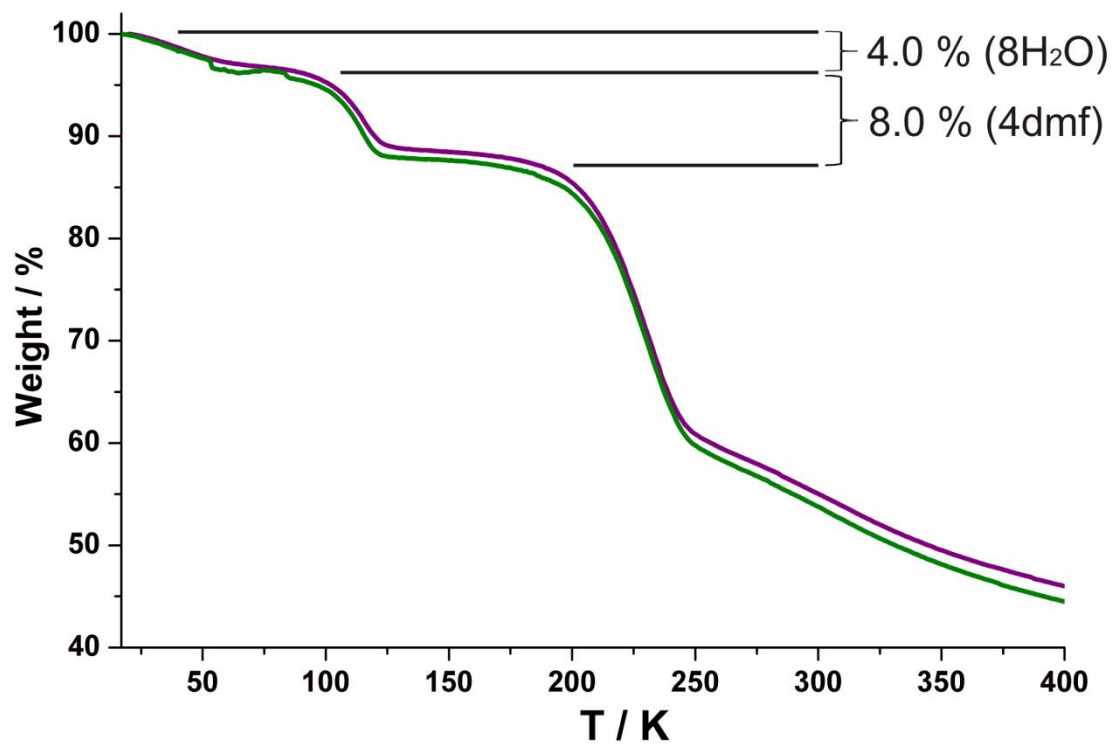
Fig. S1 TGA curves for **1**-(*RR*) (green) and **1**-(*SS*) (violet) with the marking of weight loss connected with the remove of non-coordinated water (first step, 4.0%) and four molecules of N,N-dimethylformamide (one solvent and three coordinated to Eu^{III} centers; second step, 8.0%).

Table S1 Crystal Data and Structure Refinement for **1**-(*RR*) and **1**-(*SS*)

compound		**1**-(*RR*)	**1**-(*SS*)
method		single-crystal XRD	single-crystal XRD
formula		$Eu_3W_3C_{114}H_{147}N_{46}O_{23}$	$Eu_3W_3C_{114}\,H_{147}N_{46}O_{23}$
formula weight [g·mol^{-1}]		3537.21	3537.21
T [K]		90(2)	90(2)
λ [Å]		0.71075 (Mo Kα)	0.71075 (Mo Kα)
crystal system		monoclinic	monoclinic
space group		$P2_1$	$P2_1$
unit cell	***a* [Å]**	13.1373(2)	13.1255(3)
	***b* [Å]**	18.6703(3)	18.6363(3)
	***c* [Å]**	30.2795(5)	30.2302(6)
	β [deg]	95.7920(10)	95.6620(10)
V [Å^3]		7389.0(2)	7358.6(3)
Z		2	2
calculated density [g·cm^{-3}]		1.589	1.596
absorption coefficient [cm^{-1}]		3.655	3.670
F(000)		3494	3492
crystal size [mm x mm x mm]		0.28 × 0.15 × 0.08	0.20 × 0.12 × 0.08
Θ range [deg]		3.07 – 27.48	3.08 – 27.48
limiting indices		-17 < h < 15 -24 < k <24 -39 < l < 39	-17 < h < 15 -24 < k < 24 -39 < l < 39
collected reflections		72474	72119
unique reflections		33650	33394
R$_{int}$		0.0451	0.0507
number of points		-	-
completeness [%]		99.7	99.6
refinement method		full-matrix least-squares on F^2	full-matrix least-squares on F^2
data/restraints/parameters		33650/177/1768	33394/173/1802
Flack parameter		0.010(4)	0.018(4)
GOF on F^2		1.127	1.075
final *R* indices		R$_1$ = 0.0374 [$I > 2\sigma(I)$] wR$_2$ = 0.0908 (all data)	R$_1$ = 0.0410 [$I > 2\sigma(I)$] wR$_2$ = 0.0862 (all data)
largest diff peak and hole		1.087 and -1.874 e·A^{-3}	1.386 and -1.543 e·A^{-3}
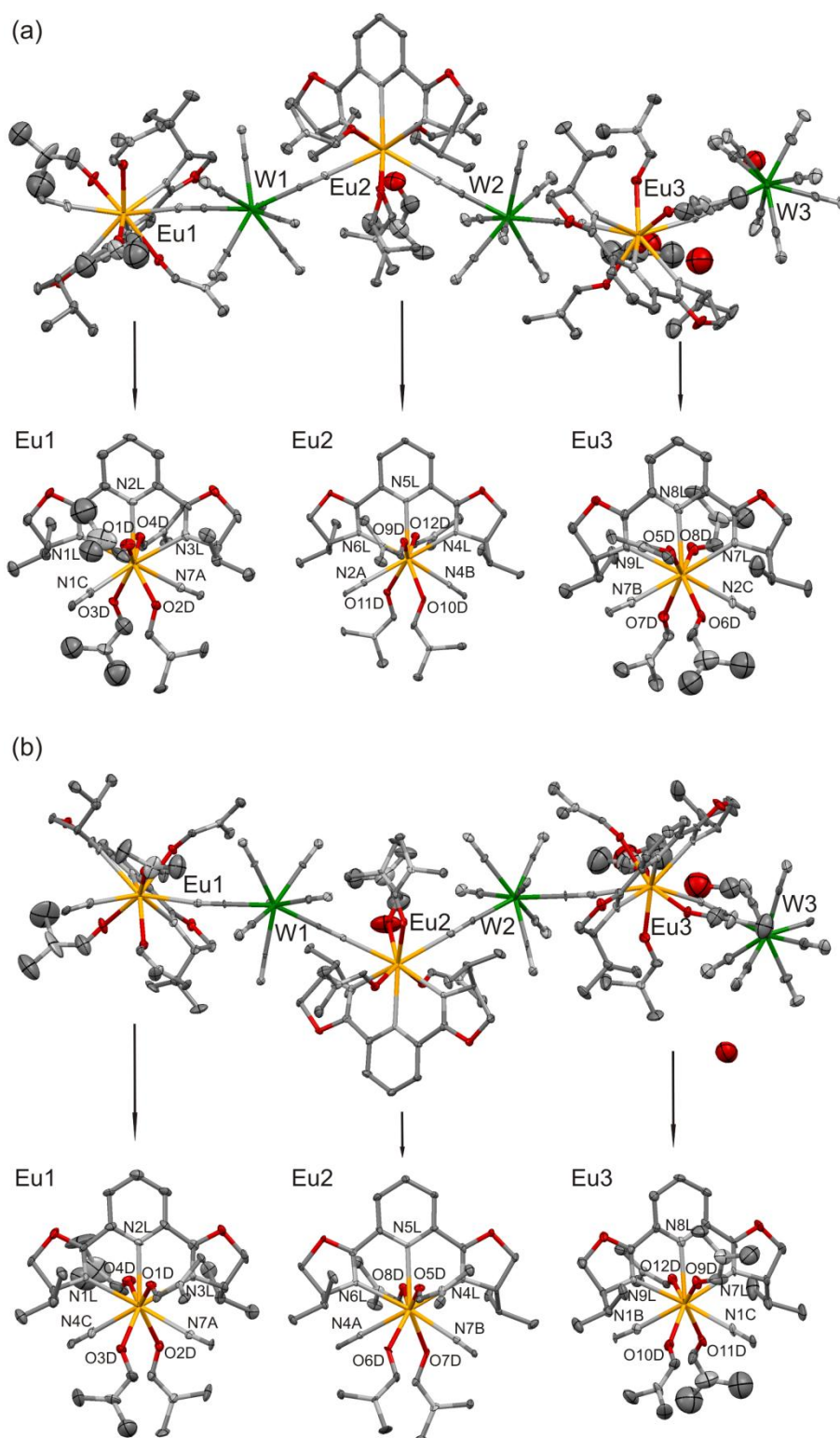
Fig. S2 The crystal structure of **1**-(*RR*) (a) and **1**-(*SS*) (b): the asymmetric units with detailed description of Eu(III) moieties. Atom spheres are shown with 50% probability ellipsoids. Hydrogen atoms are omitted for clarity. Colours: Eu – orange, W – green, O – red, C – dark grey, N – light grey.

Table S2 (part 1) Detailed structure parameters of **1**-(*RR*) and **1**-(*SS*)

Parameter	**1**-(*RR*)	**1**-(*SS*)
W1-C	2.141(6) – 2.182(5) Å	2.150(7) – 2.183(6) Å
W2-C	2.162(6) – 2.185(6) Å	2.164(6) – 2.187(6) Å
W3-C	2.146(7) – 2.187(8) Å	2.145(7) – 2.188(9) Å
C-N (W1)	1.128(7) – 1.184(8) Å	1.124(8) – 1.167(8) Å
C-N (W2)	1.137(8) – 1.176(8) Å	1.129(9) – 1.159(9) Å
C-N (W3)	1.107(10) – 1.159(11) Å	1.128(11) – 1.174(11) Å
W1-C-N	176.0(5) – 179.7(7)°	176.0(6) – 179.2(6)°
W2-C-N	176.0(5) – 179.6(6)°	174.8(6) – 178.9(7)°
W3-C-N	176.8(7) – 179.8(7)°	176.6(7) – 179.3(7)°
Eu1-W1	5.935 Å	5.929 Å
Eu1-W3	5.835 Å	5.825 Å
Eu2-W1	5.915 Å	5.916 Å
Eu2-W2	5.901 Å	5.898 Å
Eu3-W2	5.899 Å	5.895 Å
Eu3-W3	5.833 Å	5.818 Å
Eu1-N-C	172.5° (N7A-C7A) 173.3(6)° (N1C-C1C)	171.9(5)° (N7A-C7A) 171.5(6)° (N4C-C4C)
Eu2-N-C	168.6(5)° (N4B-C4B) 176.9(4)° (N2A-C2A)	168.6(5)° (N7B-C7B) 177.2(5)° (N4A-C4A)
Eu3-N-C	168.4(5)° (N2C-C2C) 173.1(5)° (N7B-C7B)	168.8(6)° (N1C-C1C) 173.4(6)° (N1B-C1B)
Eu1-N(CN)	2.626(5) Å (N7A) 2.532(5) Å (N1C)	2.616(6) Å (N7A) 2.524(6) Å (N4C)
Eu1-N(py)	2.635(5) Å (N2L)	2.626(5) Å (N2L)
Eu1-N(ox)	2.599(5) Å (N1L) 2.574(5) Å (N3L)	2.597(6) Å (N1L) 2.575(5) Å (N3L)
Eu1-O(dmf)	2.396(5) Å (O1D) 2.389(4) Å (O2D) 2.371(4) Å (O3D) 2.415(4) Å (O4D)	2.412(4) Å (O1D) 2.385(5) Å (O2D) 2.391(4) Å (O3D) 2.394(5) Å (O4D)
(CN)N-Eu1-N(CN)	126.44(17)°	126.40(18)°

Table S2 (part 2) Detailed structure parameters of **1**-(*RR*) and **1**-(*SS*)

Parameter	**1**-(*RR*)	**1**-(*SS*)
Eu2-N(CN)	2.601(5) Å (N2A) 2.606(5) Å (N4B)	2.603(5) Å (N4A) 2.614(6) Å (N7B)
Eu2-N(py)	2.641(6) Å (N5L)	2.651(5) Å (N5L)
Eu2-N(ox)	2.569(5) Å (N4L) 2.583(5) Å (N6L)	2.571(5) Å (N4L) 2.589(5) Å (N6L)
Eu2-O(dmf)	2.382(4) Å (O9D) 2.420(4) Å (O10D) 2.351(4) Å (O11D) 2.375(4) Å (O12D)	2.391(4) Å (O5D) 2.358(4) Å (O6D) 2.431(4) Å (O7D) 2.383(4) Å (O8D)
(CN)N-Eu2-N(CN)	125.96(15)°	125.73(16)°
Eu3-N(CN)	2.601(5) Å (N7B) 2.564(5) Å (N2C)	2.600(6) Å (N1B) 2.538(6) Å (N1C)
Eu3-N(py)	2.635(5) Å (N8L)	2.633(6) Å (N8L)
Eu3-N(ox)	2.577(5) Å (N7L) 2.620(5) Å (N9L)	2.591(5) Å (N7L) 2.621(5) Å (N9L)
Eu3-O(dmf)	2.441(4) Å (O5D) 2.355(5) Å (O6D) 2.336(4) Å (O7D) 2.410(5) Å (O8D)	2.421(5) Å (O9D) 2.324(5) Å (O10D) 2.356(5) Å (O11D) 2.434(5) Å (O12D)
(CN)N-Eu3-N(CN)	127.79(16)°	127.45(19)

Table S3 Results of Continuous Shape Measure analysis for $[W^V(CN)_8]^{3-}$ units in **1**-(*RR*) and **1**-(*SS*)

$[W1(CN)_8]^{3-}$	**1**-(*RR*)	**1**-(*SS*)
CSM BTP-8[§]	2.125	2.086
CSM SAPR-8	0.134	0.141
CSM DD-8	2.276	2.037
$[W2(CN)_8]^{3-}$	**1**-(*RR*)	**1**-(*SS*)
CSM BTP-8	1.687	1.700
CSM SAPR-8	0.248	0.231
CSM DD-8	2.037	2.056
$[W3(CN)_8]^{3-}$	**1**-(*RR*)	**1**-(*SS*)
CSM BTP-8	1.681	1.775
CSM SAPR-8	0.208	0.235
CSM DD-8	1.877	1.707

[§]CSM BTP-8 – the parameter corresponding to the biccapped trigonal prism;
CSM SAPR-8 – the parameter corresponding to the square antiprism;
CSM DD-8 – the parameter corresponding to the dodecahedron;
CSM = 0 for the ideal geometry and increases with the degree of distortion.[S7-S9]

Table S4 Ideal and observed dihedral δ and φ angles in $[W^V(CN)_8]^{3-}$ units in **1**-(*RR*) and **1**-(*SS*)[S10]

Complex	δ [deg]	φ [deg]
Ideal BTP-8	0; 21.8; 48.2; 48.2	14.1
Ideal SAPR-8	0; 0; 52.4; 52.4	24.5
Ideal DD-8	29.5; 29.5; 29.5; 29.5	0
$[W1(CN)_8]^{3-}$ in **1**-(*RR*)	1.2; 4.1; 52.5; 52.5	39.6
$[W1(CN)_8]^{3-}$ in **1**-(*SS*)	1.0; 4.1; 52.1; 52.6	39.3
$[W2(CN)_8]^{3-}$ in **1**-(*RR*)	3.6; 10.0; 49.2; 50.6	32.7
$[W2(CN)_8]^{3-}$ in **1**-(*SS*)	2.7; 10.9; 49.1; 51.3	34.1
$[W3(CN)_8]^{3-}$ in **1**-(*RR*)	2.4; 10.3; 48.3; 49.2	33.0
$[W3(CN)_8]^{3-}$ in **1**-(*SS*)	5.9; 10.4; 48.2; 48.5	31.8

Table S5 Results of Continuous Shape Measure analysis for $[Eu^{III}(Pr^{i}\text{-Pybox})(dmf)_4(NC)_2]^+$ units in **1**-(*RR*) and **1**-(*SS*)

$[Eu1(Pr^{i}\text{-Pybox})(dmf)_4(NC)_2]^+$	**1**-(*RR*)	**1**-(*SS*)
CSM CSAPR-9§	1.243	1.231
CSM TCTPR-9	0.970	0.963
$[Eu2(Pr^{i}\text{-Pybox})(dmf)_4(NC)_2]^+$	**1**-(*RR*)	**1**-(*SS*)
CSM CSAPR-9	1.034	1.056
CSM TCTPR-9	1.374	1.352
$[Eu3(Pr^{i}\text{-Pybox})(dmf)_4(NC)_2]^+$	**1**-(*RR*)	**1**-(*SS*)
CSM CSAPR-9	0.913	0.914
CSM TCTPR-9	1.038	1.030

§ CSM CSAPR-9 – the parameter corresponding to the capped square antiprism;
CSM TCTPR-9 – the parameter corresponding to the tricapped trigonal prism;
CSM = 0 for the ideal geometry and increases with the degree of distortion.[S7-S9]

Table S6 Ideal and observed dihedral δ angles in $[Eu^{III}(Pr^{i}\text{-Pybox})(dmf)_4(NC)_2]^+$ units of **1**-(*RR*) and **1**-(*SS*)[S11]

Edges	Ideal CSAPR-9	Ideal TCTPR-9	Eu1 **1**-(*RR*)	Eu1 **1**-(*SS*)	Eu2 **1**-(*RR*)	Eu2 **1**-(*SS*)	Eu3 **1**-(*RR*)	Eu3 **1**-(*SS*)
a	0.0	27.3	24.6	25.0	18.3	18.7	20.5	20.9
b	38.2	27.3	25.5 27.5	25.7 27.9	28.0 30.3	27.9 30.0	27.8 28.3	28.2 28.7
c	69.1	59.4	59.2 63.4	58.7 63.0	62.8 64.5	62.6 64.2	60.6 65.4	60.3 65.3
d	37.6	47.5	43.8	44.2	38.6	38.8	39.6	39.8
e	59.0	59.4	59.8 63.8	61.4 61.8	62.5 64.3	62.6 64.2	62.7 63.1	62.4 62.6
f	52.7	59.4	59.8 63.1	59.8 63.0	58.0 60.5	58.3 60.5	57.5 60.1	57.6 60.3
g	52.7	47.5	44.1 45.4	44.2 45.4	44.2 48.8	44.0 48.6	46.1 48.0	46.2 47.9
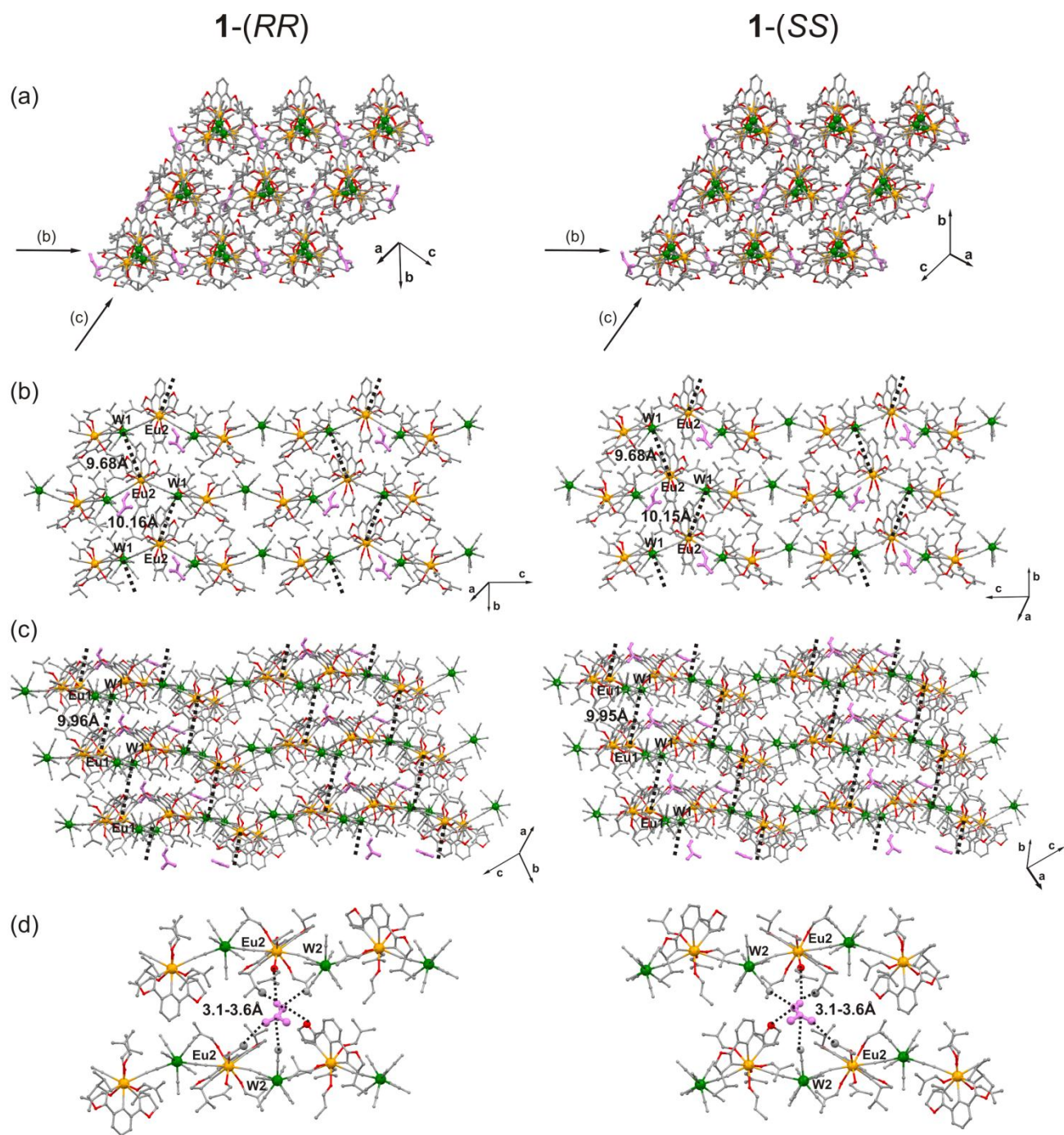
Fig. S3 The crystal structure of **1**-(*RR*) (left panel) and **1**-(*SS*) (right panel): the view along coordination chains (a), the closest metal-metal interchain contacts approximately in *bc* plane (b) and *ac* plane (c), and the enlargement of the closest contacts between molecular chains and non-coordinated dmf (d). Hydrogen atoms are omitted for clarity. Metal spheres are enlarged. Colours: Eu – orange, W – green, O – red, C – dark grey, N – light grey, atoms of non-coordinated dmf – violet.
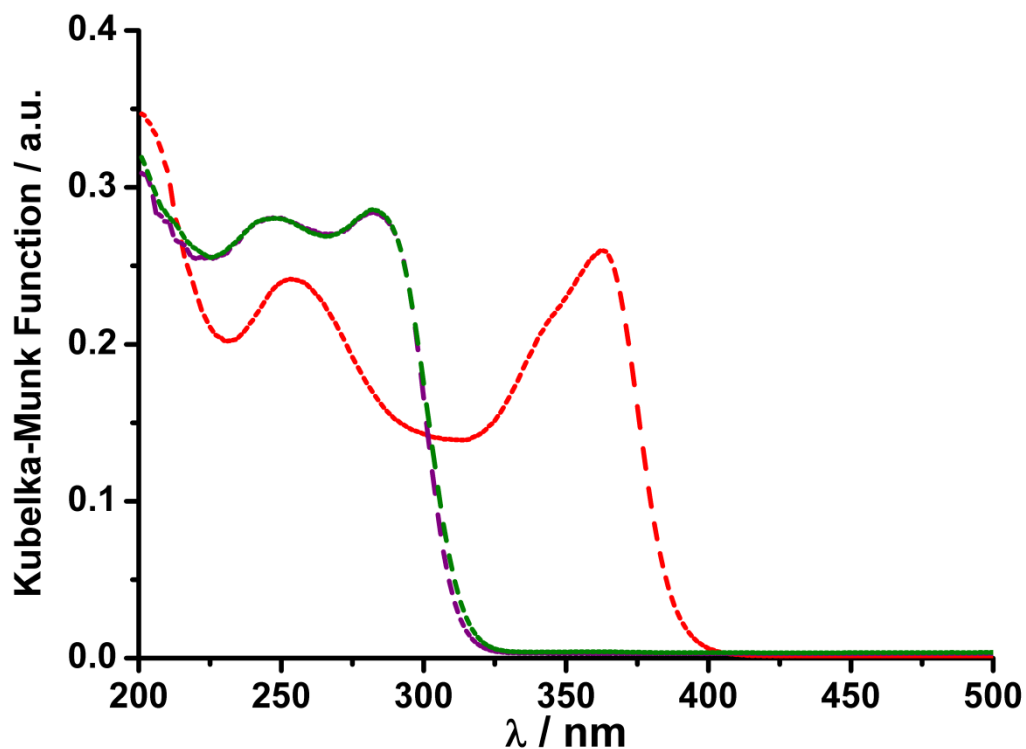
Fig. S4 UV-Vis diffuse reflectance spectra of (*RR*)-Pr^i-Pybox (green), (*SS*)-Pr^i-Pybox (violet) and TBA$_3$[W^V(CN)]$_8$ salt (red).
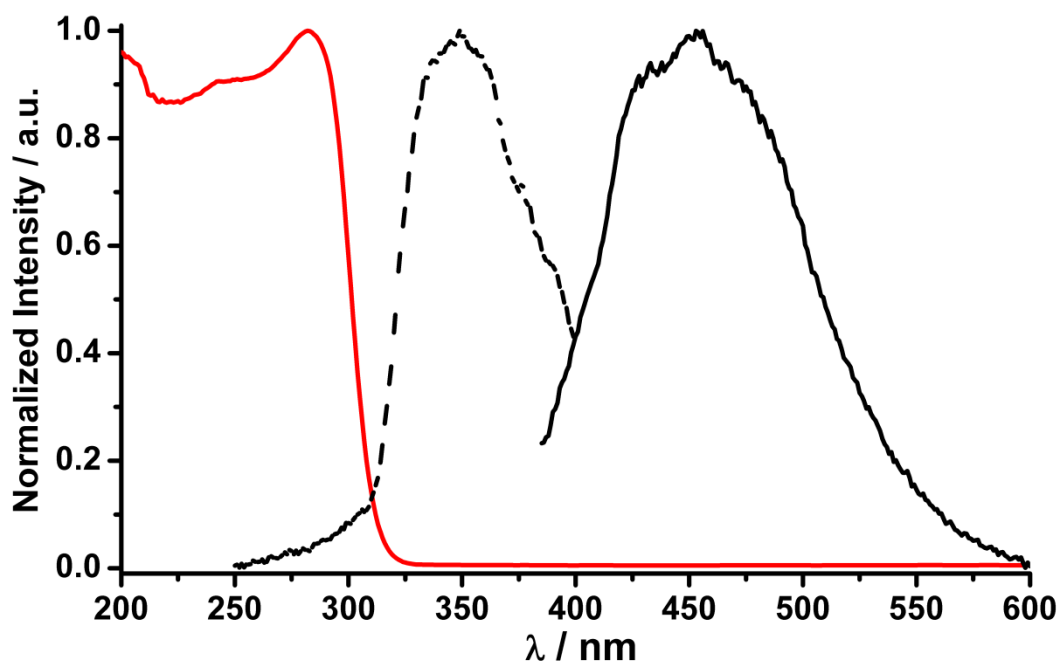
Fig. S5 Optical properties of pure Pr^i-Pybox ligand: UV-Vis absorption spectrum (red line), emission spectrum excited at 350 nm (black line) and excitation spectrum monitored around 460 nm (black dashed line).
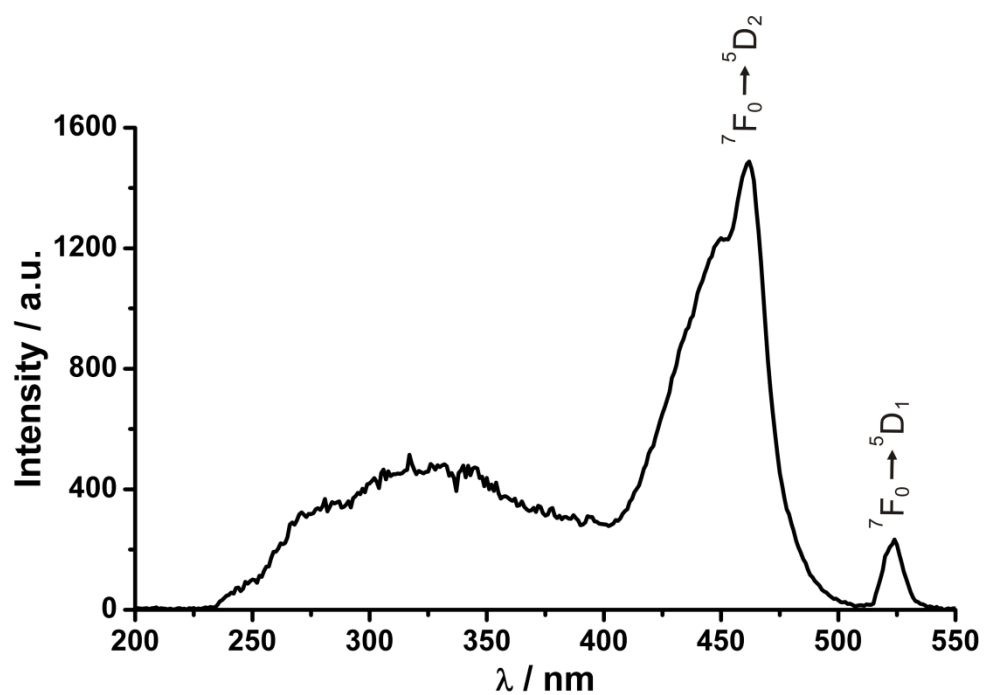
Fig. S6 Excitation spectra acquired at 77 K for **1**-(*RR*) monitored at 614 ($^5D_0 \rightarrow {}^7F_2$) and 593 ($^5D_0 \rightarrow {}^7F_1$) nm.

References to Supporting Information

(S1) R. A. Pribush and R. D. Archer, *Inorg. Chem*., 1974, **13**, 2556.

(S2) G. M. Sheldrick, *Acta Crystallogr*., 2008, **A64**, 112.

(S3) L. J. Farrugia, *J. Appl. Cryst*., 1999, **32**, 837.

(S4) O. Kahn, *Molecular Magnetism*, VCH: New York, 1993.

(S5) G. A. Bain and J. F. Berry, *J. Chem. Edu*., 2008, **85**, 532.

(S6) E. Chelebaeva, J. Long, J. Larionova, R. A. S. Ferreira, L. D. Carlos, F. A. Almeida Paz, J. B. R. Gomes, A. Trifonov, C. Guerin and Y. Guari, *Inorg. Chem*., 2012, **51**, 9005

(S7) M. Llunell, D. Casanova, J. Cirera, J. Bofill, P. Alemany, S. Alvarez, M. Pinsky and D. Avnir, *SHAPE v. 1.1b Program for the Calculation of Continuous Shape Measures of Polygonal and Polyhedral Molecular Fragments*, University of Barcelona: Barcelona, Spain, 2005.

(S8) D. Casanova, J. Cirera, M. Llunell, P. Alemany, D. Avnir and S. Alvarez, *J. Am. Chem. Soc*., 2004, **126**, 1755.

(S9) S. Alvarez, P. Alemany, D. Casanova, J. Cirera, M. Llunell and D. Avnir, *Coord. Chem. Rev*., 2005, **249**, 1693.

(S10) E. L. Muetterties and L. J. Guggenberger, *J. Am. Chem. Soc*., 1974, **96**, 1748.

(S11) B. E. Robertson, *Inorg. Chem*., 1977, **16**, 2735.

(S12) M. Kozieł, R. Pełka, M. Rams, W. Nitek and B. Sieklucka, *Inorg. Chem*., 2010, **49**, 4268.